Short Communication

A readout system for highly sensitive diamond detectors for FLASH dosimetry

Sara Pettinato [a], Giuseppe Felici [b], Lorenzo Galluzzo [b], Maria Cristina Rossi [c], Marco Girolami [d], Stefano Salvatori [a,*]

[a] *Dept. of Engineering, Niccolò Cusano University, via don Carlo Gnocchi 3, 00166 Rome, Italy*
[b] *SIT – Sordina IORT Technologies S.p.A., Aprilia, Latina, Italy*
[c] *Dept. of Industrial, Electronic, and Mechanical Engineering, Roma Tre University, Via Vito Volterra 62, 00146 Rome, Italy*
[d] *Istituto di Struttura della Materia, Consiglio Nazionale delle Ricerche (ISM–CNR), Sede Secondaria di Montelibretti, Strada Provinciale 35/D n. 9, 00010 Montelibretti, Rome, Italy*

ARTICLE INFO

ABSTRACT

Accurate dosimetry of ultra-high dose-rate beams using diamond detectors remains challenging, primarily due to the elevated photocurrent peaks exceeding the input dynamics of precision electrometers. This work aimed at demonstrating the effectiveness of compact gated-integration electronics in conditioning the current peaks (>20 mA) generated by a highly sensitive ($S \simeq 26$ nC/Gy) custom-made diamond photoconductor under electron FLASH irradiation, as well as in real-time monitoring of beam dose and dose-rate. For the emerging FLASH technology, this study provided a new perspective on using commercially available diamond dosimeters with high sensitivity, currently employed in conventional radiotherapy.

1. Introduction

In radiation therapy (RT), several preclinical and clinical studies demonstrated that the use of almost instantaneous (<200 ms) doses, delivered in a few pulses with very high dose-per-pulse (DPP) values (>1 Gy/pulse) at ultra-high dose-rates (UHDRs) (>40 Gy/s), reduced significantly the healthy tissue toxicity, while keeping the tumor response similar to that of conventional RT (i.e., with DPP < 1 mGy/pulse and dose-rate in the order of 0.01 Gy/s) [1–4]. A growing interest within the scientific community was directed towards understanding the effects induced by radiation in UHDR conditions [5–7], with the aim of establishing reliable protocols for the emerging FLASH-RT [8,9]. Consequently, substantial efforts have been dedicated to optimize the dosimetry of UHDR FLASH-beams, making it one of the pivotal focuses in current scientific research endeavors [10–17].

High-performance dosimeters capable of monitoring the intense and short electron pulses generated by medical LINACs were crucial for safe and efficient clinical translation of the innovative FLASH-RT. Ionization chambers (ICs) provided a standard reference for dosimetry in conventional RT. However, under intense electron pulses, the collection efficiency of ICs decreases, and the necessary saturation correction factors

have not been defined by standards [18]. In this context, detectors based on wide-bandgap semiconductors emerged as a valuable alternative [11,13]. Among them, diamond is extremely appealing, due to its high radiation hardness [19], tissue equivalence [20], fast response [21,22], and high volume sensitivity [23], just to mention a few properties meeting the challenging requirements for FLASH dosimetry. Some preliminary experiments confirmed the effectiveness of diamond detectors in electron FLASH dosimetry [12]. However, the dosimeter response saturated at a few Gy/pulse, mainly due to spike currents out of the electrometer input range [24]. To meet the requirements of FLASH dosimetry, diamond devices were re-designed for UHDR. By reducing both the sensitivity and the active volume of detectors, a linear response was achieved up to ~20 Gy/pulse [12,25].

Here we proposed a prototypal detection system employing a synchronous integration technique able to efficiently acquire the high photocurrent peaks (up to 24 mA) generated by a photoconductive diamond detector (active volume 3.5 mm³) irradiated by intense pulsed electron beams. Characterizations were performed at different DPP values, pulse widths, and pulse repetition frequencies (PRFs), demonstrating the effectiveness of the proposed prototype in real-time FLASH dosimetry.

---

2. Materials and methods

2.1. Detector fabrication

As shown in Fig. 1(a), the dosimeter was based on a $4.5 \times 4.5 \times 0.5$ mm^3 single crystal (1 0 0)-oriented CVD-diamond sample (Element Six) with two 200 nm-thick Ag dots (diameter 3 mm) deposited on the two sides of the sample by thermal evaporation. A 1.6 m-long triaxial cable was employed for the connection of detector contacts to the acquisition electronics. The device was encapsulated in a polymethyl methacrylate (PMMA) cylinder (diameter 1 cm, length 5 cm) filled with epoxy resin (Epotek, 301) (Fig. 1(b)). A detailed description of the device fabrication workflow was reported in [26].

2.2. Experimental setup

Measurements under high DPP electrons were performed with an ElectronFlash (named eFlash in the following) research-dedicated LINAC (SIT-Sordina IORT Technologies S.p.A, Aprilia, Italy) with the setup shown in Fig. 1(c). The diamond dosimeter, biased at only 2 V, was placed into a PMMA phantom at a depth of 2.5 cm (Fig. 1(d)). The dosimeter head was positioned at the center of the end side of a PMMA cylindrical applicator (wall thickness 5 mm, inner diameter 10 cm, and length 100 cm), with the 4.5×4.5 mm^2 diamond sides perpendicular to the beam direction. The eFlash console displayed and saved the DPP value for each electron pulse, evaluated by the pulsed current induced by the electron beam in the AC current transformer (ACCT, Bergoz Instrumentation) located immediately outside the beam exit window [27,28].

The dosimeter response as a function of the delivered DPP values, representing the dosimeter sensitivity, was measured in the range 0.5–4.6 Gy/pulse at PRF = 10 Hz, for both 7 MeV and 9 MeV pulsed electrons. To evaluate the dose-rate dependence, the eFlash was set to deliver 9 MeV electron pulses (width 4 μs) at different PRFs in the range 5–240 Hz (i.e. an effective dose-rate from 40 to 960 Gy/s). Conversely, to assess the real-time monitoring capability of the prototype, tests were carried out with the eFlash producing 5 pulses (4 μs wide) at 9 MeV, i.e. delivering a total dose of 20 Gy within ~17 ms (PRF = 240 Hz).

2.3. Readout electronics

At each electron pulse, the eFlash provided a trigger-out signal, exploited by a specifically developed gated-integrator (GI) [14,29,30] to perform synchronous integration of the photocurrent peaks generated by the diamond dosimeter. The eFlash was set to generate the trigger-out pulse 12 μs before the electron-packet emission. As outlined in the Supplementary material 1, at each trigger rising edge, the instrument acquired the charge induced by the incident pulse and collected by the detector. After a reset, the GI performed a second integration to assess potential contributions from leakage current, thereby improving the measurement accuracy. Finally, data were sent to a computer and the system waited for a new trigger.

A feedback capacitor of 22 nF nominal value (22.15 nF of effective value as found by the calibration procedure described in the Supplementary material 2) was used for the integrator in order to acquire the high photocurrent peaks generated by the dosimeter. In Fig. 1(e), an example of the front-end output voltage (blue trace) recorded for a 7 MeV 3.5 μs-wide pulse is shown. The figure also reported the trigger-out (black trace) occurring 12 μs before the ACCT peak signal (red trace) of the eFlash. The output voltage of the integrator settled to a stable value few microseconds after the end of the electron pulse. In this example, the increase of the GI output was about 1.5 V, corresponding to a collected charge of ~33 nC (see y-axis on the right of Fig. 1(e)), i.e, an average photocurrent of ~10 mA.

The GI was set to perform the signal integration in the period 5–20 μs after the trigger rising-edge. The implemented 12-bit analog-to-digital converter (ADC) then acquired the signal in the following 60 μs, recording 16 samples and then calculating both the mean value and the
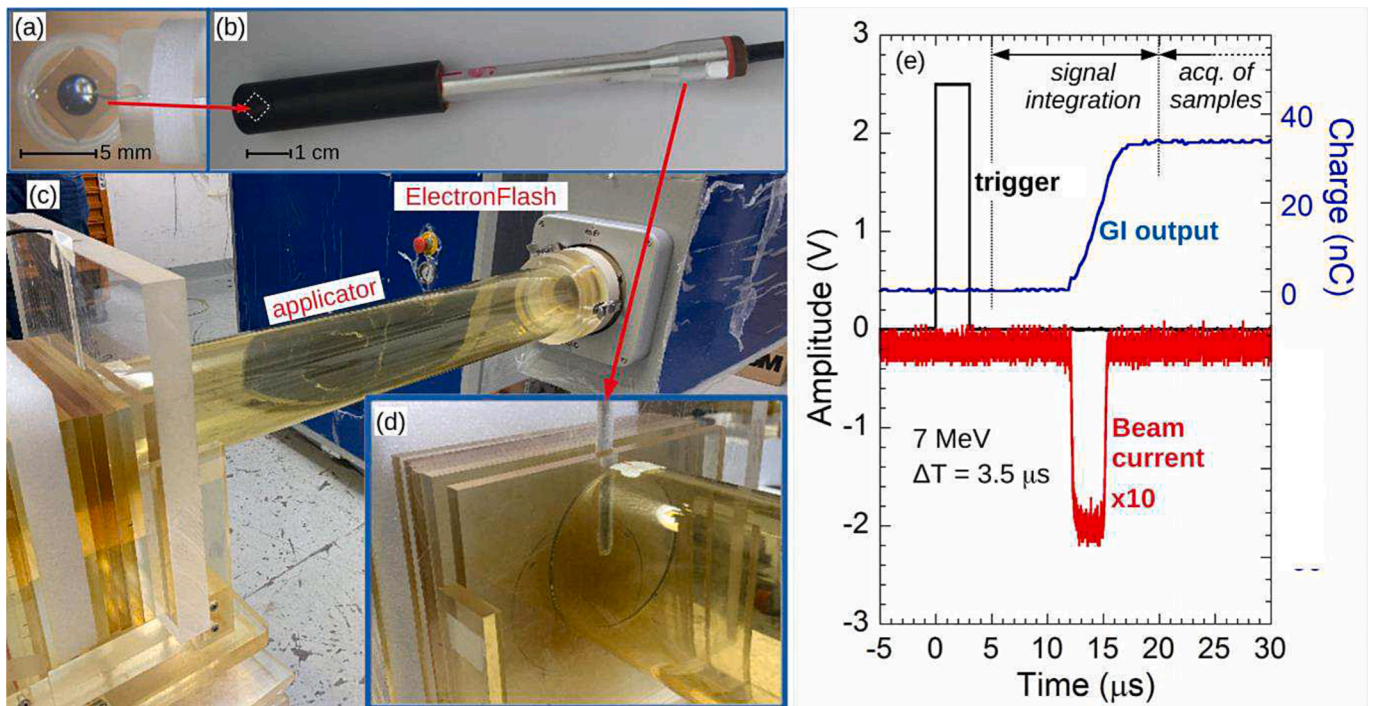

Fig. 1. (a) Picture of the diamond detector with contacts on the two sides before device encapsulation. (b) The dosimeter after the encapsulation in a hermetic PMMA enclosure. (c) ElectronFlash head with the cylindrical applicator (diameter 10 cm, length 100 cm). (d) Detail of the dosimeter immersed in a solid PMMA phantom at a depth of 2.5 cm. (e) GI output voltage (blue trace) and ACCT signal (red trace) as acquired by a digital oscilloscope. The origin of the time axis corresponds to the rising edge of the trigger signal (black trace). (For interpretation of the references to colour in this figure legend, the reader is referred to the web version of this article.)
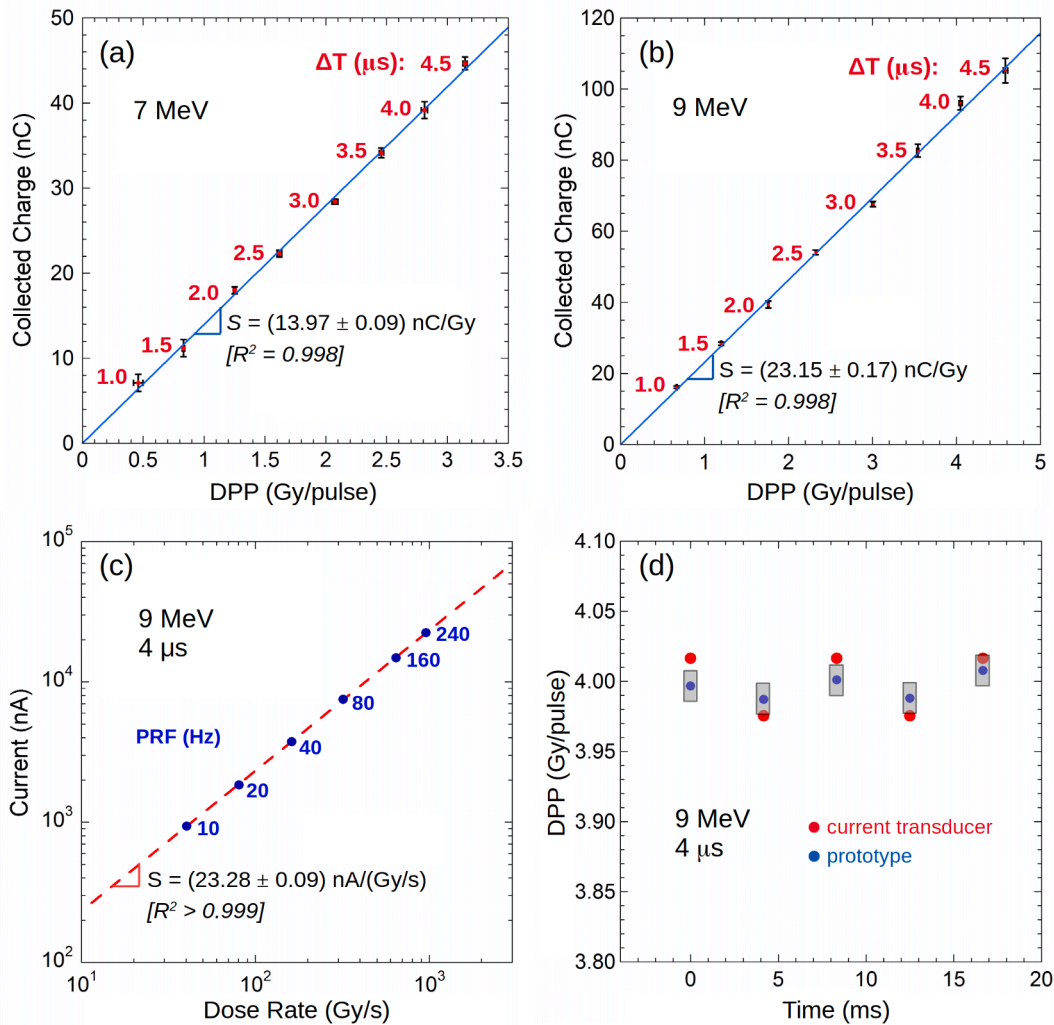
Fig. 2. Collected charge as a function of delivered DPP for (a) 7 MeV and (b) 9 MeV electrons. Each point indicates the signal averaged on ten pulses with error bars representing the standard deviation. The pulse width is reported near each point. Continuous lines are the linear best fits to data. (c) Photocurrent as a function of the effective dose-rate for 9 MeV electrons (4 μs) in the range 40–960 Gy/s (PRF ranging from 10 Hz to 240 Hz). Each point indicates the signal averaged on ten samples (error bars are smaller than symbols). Dashed line is the best linear fit to data. (d) Comparison between DPP values recorded by the ACCT of the eFlash (red circles) and by the prototypal detection system proposed in this work (blue circles). Blue circles are the mean value of the DPP calculated assuming a detector sensitivity of 23.2 nC/Gy (see Fig. 2(b)), whereas the height of the gray rectangles represents the measurement uncertainty calculated as the peak-to-peak dispersion of the 16 recorded samples of each pulse. (For interpretation of the references to colour in this figure legend, the reader is referred to the web version of this article.)

peak-to-peak dispersion of the charge collected by the detector at each eFlash pulse. Finally, for pulse-by-pulse monitoring, the GI was programmed to calculate the delivered DPP values using the detector sensitivity evaluated by preliminary characterizations.

3. Results

The characteristics of the charge collected by the dosimeter as a function of the delivered DPP values recorded by the eFlash are shown in Fig. 2(a) and (b). A very good linearity was found ($R^2 = 0.998$), with sensitivities represented by the slopes equal to 13.97 nC/Gy for 7 MeV electrons and 23.15 nC/Gy for 9 MeV electrons. The photocurrent values as a function of the effective dose-rate (equal to DPP × PRF) are reported in Fig. 2(c). Data showed excellent linearity ($R^2 > 0.999$) with a slope consistent with the results of Fig. 2(b).

Considering the detector sensitivity (23.15 nC/Gy) evaluated from the data in Fig. 2(b), the recorded values reported in Fig. 2(d) for a 20 Gy dose delivered with 5 pulses at 9 MeV showed a difference of only ±0.5% between the eFlash and the prototype.

4. Discussion

The results showed an excellent response linearity with a DPP up to ~4.6 Gy/pulse for the implemented prototype, which is independent of the dose-rate in the investigated range from 40 to 960 Gy/s. In addition, the diamond photoresponse did not show any degradation during the measurement sessions, even after the absorption of a total dose > 2 kGy as recorded by the eFlash, thus highlighting excellent radiation hardness.

The ratio between the slopes of linear best fits of data of Fig. 2(a) and (b) was consistent with the ratio between the percentage of depth-dose (PDD) values in the PMMA phantom at a depth of 25 mm for 7 MeV electrons (PDD ≃ 52%) and 9 MeV electrons (PDD ≃ 89%) [25]. Therefore, the sensitivity values were (26.9 ± 0.2) nC/Gy at 7 MeV and (26.3 ± 0.2) nC/Gy at 9 MeV, calculated as $S = S(E) / PDD(d,E)$, with $S(E)$ the sensitivity and $PDD(E,d)$ the percentage of depth-dose for electrons with energy E at a depth $d = 25$ mm in the PMMA phantom. These findings highlighted the high sensitivity of the detector used in this study. In addition, such an investigation clearly confirmed the suitability of diamond photoconductors for FLASH dosimetry. The

technology for fabricating the diamond photoconductor was simpler and more cost-effective than that required for manufacturing a diamond Schottky-diode. Although a bias voltage was required for carrier collection, the high detector sensitivity enabled low bias-voltage operation (a few Volts) under the intense radiation beams in FLASH-RT.

The designed front-end efficiently acquired input current peaks up to 24 mA (see Fig. S4), a value thirty times higher than those recently reported for an optimized diamond photodiode [13] under experimental conditions similar to those used in the present work. As a matter of fact, the proposed electronics featured a significantly wider input range compared to precision standard electrometers (typically operating in the range of a few hundred microamperes), thereby eliminating the need for attenuation stages [24].

It is worth highlighting that the proposed instrument enabled the use of a highly sensitive diamond device, making it particularly suitable for interfacing with both the established PTW-microDiamond dosimeter (S = 1 nC/Gy) [31], commonly employed in dosimetry for conventional RT, and the recently introduced PTW-flashDiamond for UHDR beams [32]. Indeed, the input dynamics of the GI can be tailored to the specific dosimeter's sensitivity by selecting the proper integrating capacitance and gain factor of the front-end (see Tab. S1). This assures optimal signal conditioning that fully exploits the input dynamics of the readout electronics. In addition, it is important to stress here that the electronic prototype completed the acquisition phases (integration, analog-to-digital conversion, processing, and data transfer) within 580 μs (see Fig. S1(b)), thus allowing for pulse-by-pulse monitoring up to PRFs of 1.7 kHz. The timing circuitry implemented by a microcontroller (Fig. S1) ensured high flexibility: integration may be indeed extended up to hundreds of milliseconds, therefore allowing for the acquisition of pulses with duration in the ms range. The adopted synchronous detection technique, exploiting the beam pulse trigger signal from the LINAC, significantly improved the system accuracy at the expense of an increased connection complexity compared to the use of a standard electrometer. However, all experiments were carried out with the instrument located in the bunker where the LINAC was installed, limiting the length of the detector cable (i.e. its capacitance), thus ensuring the reliability of the detection system even at very-high PRFs.

Two key upgrades for the comprehensive diagnostics of UHDR beams can be highlighted in the proposed prototype: *(i)* measuring the pulse duration to evaluate the instantaneous dose-rate of each pulse, and *(ii)* validating the instrument with commercial dosimeters (e.g., the PTW-microDiamond). Nevertheless, all-carbon detectors based on diamond samples [33–35], with sputter-deposited or laser-induced graphitic contacts better fulfill the tissue equivalence requirement for radiotherapy dosimetry and would offer a valuable alternative to eliminate the possible spurious signals induced by secondary electrons emitted by metallic contacts [36]. Furthermore, we would like to emphasize that the implemented measurement method may mitigate the detrimental effects of non-linear conduction mechanisms induced by structural defects distributed within the active volume of the detectors [37], as expected for laser-processed diamond samples [34,38].

In conclusion, our work marked the first implementation of gated-integration technique for the real-time monitoring of high current peaks generated by a diamond detector under intense electron beams. One notable advantage was restricting the measurement of the collected charge to the time period around the incident pulse, ensuring optimal signal-to-noise ratio. Additionally, the versatility of the proposed instrument should allow the use of established commercial diamond dosimeters for conventional RT, even in the context of FLASH dosimetry.

CRediT authorship contribution statement

Sara Pettinato: Conceptualization, Methodology, Software, Formal analysis, Investigation, Writing – original draft. **Giuseppe Felici:** Validation, Resources, Writing – review & editing. **Lorenzo Galluzzo:** Visualization, Writing – review & editing. **Maria Cristina Rossi:** Visualization, Supervision, Writing – review & editing. **Marco Girolami:** Visualization, Writing – review & editing. **Stefano Salvatori:** Conceptualization, Methodology, Validation, Data curation, Writing – original draft, Writing – review & editing, Supervision.

Declaration of competing interest

The authors declare the following financial interests/personal relationships which may be considered as potential competing interests: Giuseppe Felici is a SIT S.p.A. shareholder. Lorenzo Galluzzo is an employee at SIT S.p.A.

Appendix A. Supplementary data

Supplementary data to this article can be found online at https://doi.org/10.1016/j.phro.2024.100538.

References

[1] Favaudon V, Caplier L, Monceau V, Pouzoulet F, Sayarath M, Fouillade C, et al. Ultrahigh dose-rate FLASH irradiation increases the differential response between normal and tumor tissue in mice. Sci Transl Med 2014;6:245ra93. https://doi.org/10.1126/scitranslmed.3008973.

[2] Vozenin MC, De Fornel P, Petersson K, Favaudon V, Jaccard M, Germond JF, et al. The advantage of FLASH radiotherapy confirmed in mini-pig and cat-cancer patients. Clin Cancer Res 2019;25:35–42. https://doi.org/10.1158/1078-0432.CCR-17-3375.

[3] Wright MD, Romanelli P, Bravin A, Le Duc G, Brauer-Krisch E, Requardt H, et al. Non-conventional ultra-high dose rate (FLASH) microbeam radiotherapy provides superior normal tissue sparing in rat lung compared to non-conventional ultra-high dose rate (FLASH) radiotherapy. Cureus 2021;13:e19317. https://doi.org/10.7759/cureus.19317.

[4] Bourhis J, Sozzi WJ, Jorge PG, Gaide O, Bailat C, Duclos F, et al. Treatment of a first patient with FLASH-radiotherapy. Radiother Oncol 2019;139:18–22. https://doi.org/10.1016/j.radonc.2019.06.019.

[5] Montay-Gruel P, Acharya MM, Petersson K, Alikhani L, Yakkala C, Allen BD, et al. Long-term neurocognitive benefits of FLASH radiotherapy driven by reduced reactive oxygen species. Proc Natl Acad Sci 2019;166:10943–51. https://doi.org/10.1073/pnas.1901777116.

[6] Pawelke J, Brand M, Hans S, Hideghéty K, Karsch L, Lessmann E, et al. Electron dose rate and oxygen depletion protect zebrafish embryos from radiation damage. Radiother Oncol 2021;158:7–12. https://doi.org/10.1016/j.radonc.2021.02.003.

[7] Jansen J, Knoll J, Beyreuther E, Pawelke J, Skuza R, Hanley R, et al. Does FLASH deplete oxygen? Experimental evaluation for photons, protons, and carbon ions. Med Phys 2021;48:3982–90. https://doi.org/10.1002/mp.14917.

[8] Schüler E, Acharya M, Montay-Gruel P, Loo BW, Vozenin MC, Maxim PG. Ultra-high dose rate electron beams and the FLASH effect: from preclinical evidence to a new radiotherapy paradigm. Med Phys 2022;49:2082–95. https://doi.org/10.1002/mp.15442.

[9] Romano F, Bailat C, Jorge PG, Lerch MLF, Darafsheh A. Ultra-high dose rate dosimetry: challenges and opportunities for FLASH radiation therapy. Med Phys 2022;49:4912–32. https://doi.org/10.1002/mp.15649.

[10] Di Martino F, Del Sarto D, Bisogni MG, Capaccioli S, Galante F, Gasperini A, et al. A new solution for UHDP and UHDR (Flash) measurements: Theory and conceptual design of ALLS chamber. Phys Med 2022;102:9–18. https://doi.org/10.1016/j.ejmp.2022.08.010.

[11] Romano F, Milluzzo G, Di Martino F, D'Oca MC, Felici G, Galante F, et al. First characterization of novel silicon carbide detectors with ultra-high dose rate electron beams for FLASH radiotherapy. Appl Sci 2023;13:2986. https://doi.org/10.3390/app13052986.

[12] Marinelli M, Felici G, Galante F, Gasparini A, Giuliano L, Heinrich S, et al. Design, realization, and characterization of a novel diamond detector prototype for FLASH radiotherapy dosimetry. Med Phys 2022;49:1902–10. https://doi.org/10.1002/mp.15473.

[13] Marinelli M, Di Martino F, Del Sarto D, Pensavalle JH, Felici G, Giunti L, et al. A diamond detector based dosimetric system for instantaneous dose rate measurements in FLASH electron beams. Phys Med Biol 2023;68:175011. https://doi.org/10.1088/1361-6560/acead0.

[14] Pettinato S, Girolami M, Rossi MC, Barettin D, Salvatori S. Toward Single-Pulse Monitoring for FLASH Radiotherapy. In Cocorullo G, Crupi F, Limiti E, editors. Lect Notes Electr Eng, vol 1005, Switzerland: Springer, Cham; 2023. pp. 134–139. https://doi.org/10.1007/978-3-031-26066-7_21.

[15] Pettinato S, Salvatori S. Diamond-based detection systems for tomorrow's precision dosimetry. Nucl Instrum Methods Phys Res A 2024;1059:168974. https://doi.org/10.1016/j.nima.2023.168974.

[16] Cotterill J, Flynn S, Thomas R, Subiel A, Lee N, Shipley D, et al. Monte Carlo modelling of a prototype small-body portable graphite calorimeter for ultra-high dose rate proton beams. Phys Imaging Radiat Oncol 2023;28:100506. https://doi.org/10.1016/j.phro.2023.100506.

[17] Horst F. Calorimetry as a tool to improve the dosimetric accuracy in novel radiotherapy modalities. Phys Imaging Radiat Oncol 2023;28:100516. https://doi.org/10.1016/j.phro.2023.100516.

[18] Subiel A, Moskvin V, Welsh GH, Cipiccia S, Rebored D, DesRosiers C, et al. Challenges of dosimetry of ultra-short pulsed very high energy electron beams. Phys Med 2017;42:327–31. https://doi.org/10.1016/j.ejmp.2017.04.029.

[19] Shimaoka T, Koizumi S, Kaneko JH. Recent progress in diamond radiation detectors. Functional Diam 2021;1:205–20. https://doi.org/10.1080/26941112.2021.2017758.

[20] Górka B, Fernández-Varea JM, Panettieri V, Nilsson B. Optimization of a tissue-equivalent CVD-diamond dosimeter for radiotherapy using the Monte Carlo code PENELOPE. Nucl Instrum Methods Phys Res A 2008;593:578–87. https://doi.org/10.1016/j.nima.2008.05.044.

[21] Salvatori S, Girolami M, Oliva P, Conte G, Bolshakov A, Ralchenko VG, et al. Diamond device architectures for UV laser monitoring. Laser Phys 2016;26:84005. https://doi.org/10.1088/1054-660X/26/8/084005.

[22] Girolami M, Allegrini P, Conte G, Trucchi DM, Ralchenko VG, Salvatori S. Diamond detectors for UV and X-ray source imaging. IEEE Electron Device Lett 2012;33:224–6. https://doi.org/10.1109/LED.2011.2176907.

[23] Talamonti C, Kanxheri K, Pallotta S, Servoli L. Diamond detectors for radiotherapy X-ray small beam dosimetry. Front Phys 2021;9:632299. https://doi.org/10.3389/fphy.2021.632299.

[24] Kranzer R, Schüller A, Bourgouin A, Hackel T, Poppinga D, Lapp M, et al. Response of diamond detectors in ultra-high dose-per-pulse electron beams for dosimetry at FLASH radiotherapy. Phys Med Biol 2022;67:075002. https://doi.org/10.1088/1361-6560/ac594e.

[25] Verona Rinati G, Felici G, Galante F, Gasparini A, Kranzer R, Mariani G, et al. Application of a novel diamond detector for commissioning of FLASH radiotherapy electron beams. Med Phys 2022;49:5513–22. https://doi.org/10.1002/mp.15782.

[26] Pettinato S, Girolami M, Stravato A, Serpente V, Musio D, Rossi MC, et al. A highly versatile X-ray and electron beam diamond dosimeter for radiation therapy and protection. Mater 2023;16:824. https://doi.org/10.3390/ma16020824.

[27] Oesterle R, Gonçalves JP, Grilj V, Bourhis J, Vozenin MC, Germond JF, et al. Implementation and validation of a beam-current transformer on a medical pulsed electron beam LINAC for FLASH-RT beam monitoring. J Appl Clin Med Phys 2021;22:165–71. https://doi.org/10.1002/acm2.13433.

[28] Di Martino F, Del Sarto D, Bass G, Capaccioli S, Celentano M, Coves D, et al. Architecture, flexibility and performance of a special electron linac dedicated to Flash radiotherapy research: electronFlash with a triode gun of the centro pisano flash radiotherapy research (CPFR). Front Phys 2023;11:1268310. https://doi.org/10.3389/fphy.2023.1268310.

[29] Pettinato S, Girolami M, Rossi MC, Salvatori S. Accurate signal conditioning for pulsed-current synchronous measurements. Sens 2022;22:5360. https://doi.org/10.3390/s22145360.

[30] Pettinato S, Girolami M, Olivieri R, Stravato A, Caruso C, Salvatori S. Time-resolved dosimetry of pulsed photon beams for radiotherapy based on diamond detector. IEEE Sens J 2022;22:12348–56. https://doi.org/10.1109/JSEN.2022.3173892.

[31] microDiamond Detector TW60019. https://www.ptwdosimetry.com/en/products/microdiamond [accessed 13 January 2024].

[32] flashDiamond Detector T60025. https://www.ptwdosimetry.com/en/products/flashdiamond-detector [accessed 13 January 2024].

[33] Girolami M, Criante L, Di Fonzo F, Lo Turco S, Mezzetti A, Notargiacomo A, et al. Graphite distributed electrodes for diamond-based photon-enhanced thermionic emission solar cells. Carbon 2017;111:48–53. https://doi.org/10.1016/j.carbon.2016.09.061.

[34] Rossi MC, Salvatori S, Conte G, Kononenko T, Valentini V. Phase transition, structural defects and stress development in superficial and buried regions of femtosecond laser modified diamond. Opt Mater 2019;96:109214. https://doi.org/10.1016/j.optmat.2019.109214.

[35] Khomich AA, Ashikkalieva KK, Bolshakov AP, Kononenko TV, Ralchenko VG, Konov VI, et al. Very long laser-induced graphitic pillars buried in single-crystal CVD-diamond for 3D detectors realization. Diam Relat Mater 2018;90:84–92. https://doi.org/10.1016/j.diamond.2018.10.006.

[36] Awan TI, Bashir A, Tehseen A, Bibi S. Electrons in nanostructures. In: Awan TI, Bashir A, Tehseen A, editors. Chem Nanomater. Amsterdam: Elsevier; 2020. p. 179–206. https://doi.org/10.1016/B978-0-12-818908-5.00007-X.

[37] Salvatori S, Pettinato S, Girolami M, Trucchi DM, Rossi MC. Improving the performance of pulsed-current detectors for pulsed X-ray dosimetry using the synchronous detection technique. IEEE Trans Electron Devices 2023;70:2330–5. https://doi.org/10.1109/TED.2023.3250390.

[38] Salvatori S, Pettinato S, Girolami M, Kononenko T, Ralchenko V, Rossi MC. The synchronous detection technique for the accurate monitoring of high-energy pulsed X-rays. Nucl Instrum Methods Phys Res A 2024;1059:168954. https://doi.org/10.1016/j.nima.2023.168954.